Photoinduced Optical Transparency in Dye-Sensitized Solar Cells Containing Graphene Nanoribbons

ARTICLE *in* THE JOURNAL OF PHYSICAL CHEMISTRY C · NOVEMBER 2011

Impact Factor: 4.77 · DOI: 10.1021/jp2069946

7 AUTHORS, INCLUDING:

Josef Velten
University of Texas at Dallas
8 PUBLICATIONS **71** CITATIONS

SEE PROFILE

Anvar Zakhidov
University of Texas at Dallas
329 PUBLICATIONS **14,417** CITATIONS

SEE PROFILE

THE JOURNAL OF PHYSICAL CHEMISTRY C

ARTICLE

pubs.acs.org/JPCC

Photoinduced Optical Transparency in Dye-Sensitized Solar Cells Containing Graphene Nanoribbons

Josef A. Velten,[†] Javier Carretero-González,[†,‡] Elizabeth Castillo-Martínez,[†,‡] Julia Bykova,[†] Alex Cook,[†] Ray Baughman,[†] and Anvar Zakhidov*[,†]

[†]The Alan G. MacDiarmid NanoTech Institute, University of Texas at Dallas, Richardson, Texas 75083, United States

[‡]CIC energigune, Alava Technology Park, Albert Einstein 48—ED, CIC 01510 Miñano, Álava, Spain

ABSTRACT: We describe the use of few-layer graphene nanoribbons, either attached to counter electrodes or dispersed into electrolyte, to induce optical transparency of an iodide/triiodide redox couple in a dye-sensitized solar cell (DSSC). We then evaluate the effect of reversible bleaching of the electrolyte on the DSSC performance. This bleaching effect is related to an energy transfer from photoexcited quantum-dot-like regions to the triiodide (I_3^-) radical ions in the electrolyte, saturating their absorption in the visible optical range. DSSC power conversion efficiency using few-layer graphene nanoribbons at the counter electrode (5.8%) did not deteriorate when the electrolyte became optically transparent. The increased transparency of the electrolyte resulted in a decreased photocurrent density (from 17.6 to 14.2 mA/cm^2), an unchanged open circuit voltage of 750 mV, and a slightly increased fill factor (from 0.45 to 0.55). When the few-layer graphene nanoribbons were introduced into the electrolyte directly by ultrasonication, a semitransparent DSSC was found to have increased its power conversion efficiency in an optically inverted setup from 5.75% to 7.01%, arising from an increase in photocurrent from 9.9 to 12.1 mA/cm^2. This significant photocurrent increase demonstrates that the effect of electrolyte bleaching can be used for further improving power conversion efficiency for inverted and tandem DSSCs, in which light has to pass through the electrolyte to generate photocurrent on one or more photocells.

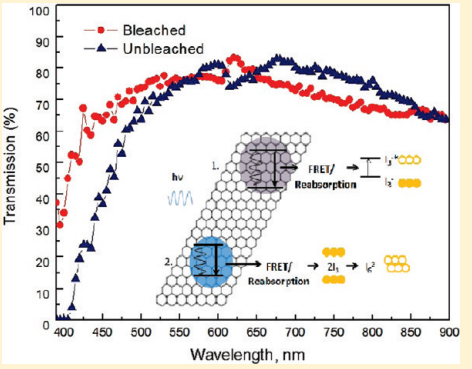

1. INTRODUCTION

Dye-sensitized solar cells (DSSCs) are a type of nanostructured solar cell based on a photoelectrochemical reaction by charge injection from an excited dye to a photoelectrode. Their basic components incorporate nanostructures of TiO_2, a photosensitive dye, a redox couple for charge mediation, and a platinized counter electrode.[1] The highest reported power conversion efficiencies are for DSSCs that use the iodine/triiodide (I^-/I_3^-) redox couple, which absorbs some of the useful light in the visible range (390−750 nm), thereby shading the photoactive layer.[2] This shading may become a major issue for optically inverted[3] and tandem DSSCs[4] in which light must pass through the electrolyte to reach the photoelectrode. Alternative chemistries for electrolytes that are more transparent have been devised,[5−7] but these more transparent electrolytes have lower power conversion efficiencies than the standard I^-/I_3^- redox couple.

We have observed that we can induce a reversible increase of transparency of the I^-/I_3^--based electrolyte by using few-layered graphene nanoribbons (GNRs) in the DSSC. This is surprising, since there have been no reports of similar photobleaching induced by other tested carbon nanostructures, such as single-walled carbon nanotubes,[8] multiwalled carbon nanotubes,[9] graphene flakes,[10] and carbon black.[11]

In this paper we report reversible photoinduced modification of the absorbance spectrum for an electrolyte utilizing an I^-/I_3^- redox couple when using thin films of a chemically and thermally reduced high-aspect-ratio GNR as a counter electrode and as an additive to the electrolyte. When applied as a counter electrode, this nonoptimized device exhibits an efficiency of over 5.8%, in addition to the photoinduced transparency of the electrolyte. In fact, the photobleaching even slightly enhances the fill factor at the expense of slightly decreased photocurrent, leaving performance nearly unchanged. This effect was tested in an optically inverted setup, where the DSSC geometry is set up in which photons enter though a transparent cathode and must travel through the electrolyte to reach a titania/dye photoelectrode, which is usually coated on an opaque substrate as a cost-savings measure. Few-layer graphene nanoribbons were then used as an additive to the electrolyte in an optically inverted setup, and the photocurrent improved by ∼2.2 mA/cm^2, an increase of over 21%. This ability to change the electrolyte's transparency by this photobleaching effect is very useful for inverted DSSCs, as any strong deviations of the iodine concentrations from the standard electrolyte will result in much poorer photovoltaic performance.[12,13]

2. EXPERIMENTAL SECTION

Synthesis of Few-Layer Graphene Nanoribbons. Vertically aligned multiwalled carbon nanotube (carbon MWNT) forests were produced by catalytic chemical vapor deposition (CVD) on

Received: July 21, 2011
Revised: October 17, 2011
Published: October 27, 2011

silicon substrates similar to what is described in another paper.[14] A 3 nm iron film was deposited on a Si wafer by e-beam evaporation to serve as the catalyst for CVD growth. The carbon MWNTs were grown at 750 °C in a CVD reactor using a C_2H_2 (5%)/H_2 (10%)/He gas mixture and a growth time of 10−15 min. The forest height measured in an optical microscope ranged from 400 to 600 um, depending on the growth time. Transmission electron microscopy (TEM) measurements indicated carbon MWNT diameters of 12−15 nm and 6−9 walls in each carbon MWNT.

The process for creating few-layer graphene nanoribbons is similar to that developed by the Tour group.[15,16] Using a 50 mL Erlenmeyer flask, 35 mg of MWNTs was dispersed in 35 mL of concentrated H_2SO_4 (ACS grade, 95−98 wt %, Merck) and stirred overnight. Then 4 mL of H_3PO_4 (ACS grade, ≥ 85 wt % in H_2O, Sigma-Aldrich) was added to the mixture of carbon nanotubes and sulfuric acid (H_2SO_4:H_3PO_4 final volume ratio of 9:1) and stirred for 15 min. Immediately thereafter, 0.34 g (8.5 wt equiv) of $KMnO_4$ (ACS grade, Merck) was added to this mixture, and the reaction was heated to 65 °C for 1 h. The reaction was stopped by placing the flask into an ice bath (∼200 mL) containing 3 mL of H_2O_2 (ACS grade, 30% in water, Fisher). The mixture was filtered over a 0.45 μm pore size poly(tetrafluoroethylene) (PTFE) membrane (Sartorius Stedim Biotech) and then successively washed and filtered twice with 200 mL of 30% HCl (ACS grade, 36.5−38%, Fisher) and 200 mL of deionized water (HPLC grade, Fisher). The resulting graphene oxide nanoribbons were first redispersed in 40 mL of deionized water (HPLC grade, Fisher) by stirring overnight and then were placed into SnakeSkin dialysis tubing (10K molecular weight cutoff (MWCO), Pierce) and dialyzed for 10 days to remove impurities from the inorganic acids and the salt employed as an oxidizing mixture. The absence of several steps of continuous sonication and ultracentrifugation during the purification of the nanoribbons was to avoid cutting of the nanoribbons, which would reduce the aspect ratio of the nanoribbons. After dialysis, the suspension of graphene oxidized nanoribbons in water was filtered through a 0.45 μm pore size PTFE membrane. The solid obtained on the filter was vacuum-dried overnight at room temperature to obtain 24 mg of product. The yield was ∼70%.

To reduce graphene oxide nanoribbons chemically, an 8 mL suspension of graphene oxide nanoribbons was dispersed in deionized water (HPLC grade, Fisher) to provide a nanotube concentration of 3 mg/mL, which was then poured into a 100 mL two-neck round-bottom flask that was equipped with a stir bar, a reflux condenser, and a septum inlet containing 72 mL of anhydrous *N*,*N*-dimethylformamide (ACS grade, 99.8%, Sigma-Aldrich). Then 4 μL of hydrazine monohydrate (ACS grade, 64−65%, Sigma-Aldrich) was added to the mixture and heated to 85 °C for overnight reflux. The reaction was cooled to room temperature and used directly to prepare the electrodes by drop-casting. Thermal reduction was performed in a 5% hydrogen/argon environment at 300 °C for 2 h, after the graphene nanoribbons were deposited onto the electrodes. Characterization of the GNR was carried out by X-ray diffraction (XRD), Raman, UV−vis, scanning electron microscopy (SEM), and TEM measurements. The XRD patterns were recorded with a Rigaku Ultima III diffractometer using Cu Kα radiation. Data were collected from 3° to 40°, 2θ, with a step size of 0.04° and 2−5 s per step. Raman spectra were recorded with a Horiba LabRAM HR spectrometer using 633 nm excitation. TEM and high-resolution TEM (HRTEM) were performed in a JEOL 2100-FEG electron microscope using an accelerating voltage of 200 kV.

Testing of the Photoluminesence Characteristics of the Few-Layer Graphene Nanoribbon. Few-layer graphene nanoribbons were deposited from solution onto a quartz slide and inserted into a cuvette containing acetonitrile, secured to the side of the cuvette facing the photoexcitation beam. Scans were completed in a PerkinElmer LS 55 luminescence spectrometer.

Dye Solar Cell Fabrication and Characterization. Fluorinated tin oxide (F:SnO_2, FTO) glass (8 Ω/square, Hartford glass) was cut and sonicated in a successive series of baths of deionized (DI) water, ethanol, acetone, and toluene for 15 min each and then set under a UV lamp for 15 min to clean the surface. After cleaning, they were immersed in a bath of a 40 mM solution of aqueous $TiCl_4$ for 30 min at 80 °C, removed, and rinsed with DI water. A TiO_2 active layer (Dyesol NR-18) was then doctor bladed onto the FTO plate surface to a thickness of approximately 10 μm and dried at 100 °C for 15 min, and then a second layer (Dyesol WER-O4) was doctor bladed on top of the transparent, active layer and dried again at 100 °C for 10 min. This substrate was then sintered for 30 min at 500 °C. For semitransparent DSSCs, the second layer of paste (Dyesol WER-O4) was not used. After this first sintering operation, the FTO plates were then immersed in a new 40 mM solution of aqueous $TiCl_4$ at 70 °C for 30 min, cleaned in DI water, and sintered a second time at 500 °C for 30 min. These plates were then cooled to 80 °C and immersed in a 1:1 ratio of acetonitrile and *tert*-butyl alcohol with 2.5×10^{-4} M *cis*-diisothiocyanatobis(2,2′-bipyridyl-4,4′-dicarboxylato)ruthenium(II) bis(tetrabutylammonium) in solution, known as N719 dye.

The counter electrode FTO plate had a small hole drilled into it for future vacuum backfilling of electrolyte, and it was cleaned in the same manner as the above working electrode. For making a platinum counter electrode, a drop of hydrogen hexachloroplatinate (diluted in 2-propanol by a 25:1 volume ratio) was spin coated at 1000 rpm for 30 s onto the cleaned substrate and then heated on a hot plate at 400 °C.

The counter electrode using graphene ribbons was fabricated by drop-casting a layer of the solution of graphene nanoribbons onto the FTO substrate, which was then dried at 50 °C for 30 min. Then the graphene nanoribbons were placed in a 5% hydrogen/argon environment, heated to 300 °C for 2 h, and allowed to slowly cool. The two plates were then sandwiched together with a 25 μm Surlyn gasket and hot pressed to melt the gasket. The electrolyte used for this test series was composed of 1-methyl-3-propylimidazolium iodide (0.6 M), iodine (0.03 M), guanidine thiocyanate (0.1 M), and 4-*tert*-butylpyridine (0.5 M) in acetonitrile. The electrolyte containing graphene ribbons was prepared by sonication of a 0.22 mg/mL concentration of graphene nanoribbons in acetonitrile and then left for 24 h to allow graphene nanoribbons not in suspension to settle to the bottom of the vial. The concentration estimated from weighing the graphene nanoribbons that did not go into suspension was approximately 0.04 mg/mL. The cells were then masked with a black permanent marker and tested on a Thermo Oriel solar simulator set at air mass (AM) 1.5 radiation with the intensity set at 100 mW/cm^2.

Measurements of transparency were taken by shining monochromatic light through an optical chopper and then through the substrate and onto a calibrated silicon photodiode (Hammamatsu). The diode was placed in parallel with a small resistor to put it in

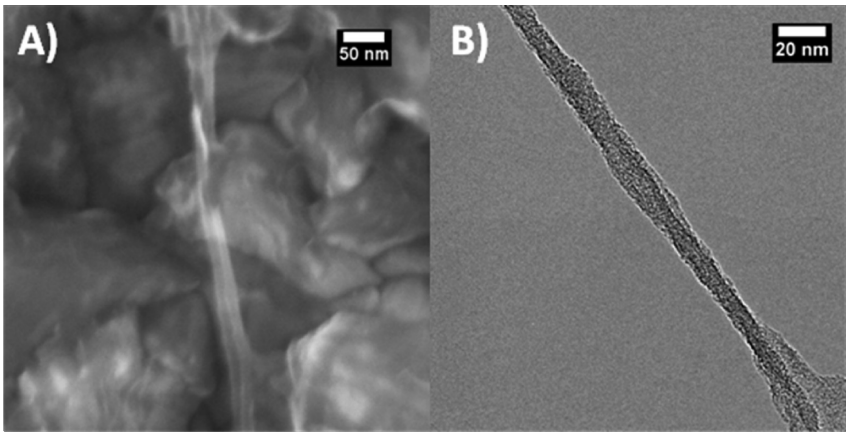

Figure 1. (A) SEM image of GNRs on an F:SnO_2 substrate. (B) TEM image showing an individual nanoribbon with a ribbon width in the range of 5−20 nm and the few stacked layers that are consistent with photoluminesence.[6]

the short circuit regime, and then the voltage across this resistor was measured by an SRS 830 lock-in amplifier. Measurements of the photobleaching effect were taken using undyed TiO_2 and a few-layer graphene nanoribbon dummy device biased by a 1.5 global (AM 1.5G) light and an electrical bias of 1.5 V (Keithley 236 SMU) to replace the driving force of the dye. This light was introduced after the chopper and was removed from the signal by the lock-in amplifier. To further remove noise caused by the light bias, several measurements were taken and averaged. Transparency was calculated by dividing the luminous power received by the photodiode with the sample in front of it by the power received with no sample in front of it.

3. RESULTS AND DISCUSSION

While the applicability of GNRs as a catalyst for the reduction of triiodide was being tested, a secondary reaction was found at this few-layer graphene nanoribbon and triiodide interface. There was a photoexcitation of the graphene nanoribbons that led to an energy transfer, either Forster resonant energy transfer (FRET) or photon reabsorption, to the triiodide at the counter electrode. This excitation leads to a photobleaching effect that is completely reversible, allowing for enhanced control of the optical properties of the DSSC.

Electrodes based on graphene nanoribbons were prepared by drop-casting the chemically reduced[17] graphene nanoribbon dispersion on top of a glass substrate with a surface layer of F:SnO_2 (FTO). Parts A and B of Figure 1 show SEM and TEM micrographs of the GNRs on an FTO substrate. The thickness of the graphene nanoribbon films can be tuned by changing the number of casting repetitions. For example, after 10 drop-castings, a ∼100 nm thick film was obtained, as measured by profilometry (Figure 1A). We maintained a high aspect ratio of the GNRs by avoiding any bath or ultrasonication step, allowing for ribbons to act as bridges between the individual crystals of the electrically conducting FTO substrate.

Raman spectroscopy was carried out to evaluate the chemical unzipping of MWNTs using a Horiba LabRAM HR spectrometer and an excitation wavelength of 633 nm. These measurements revealed a decrease in intensity for the D (1320 cm^{-1}) and G (1596 cm^{-1}) bands, as well as the overtone at around 2637 cm^{-1}, as compared with band intensities for pristine

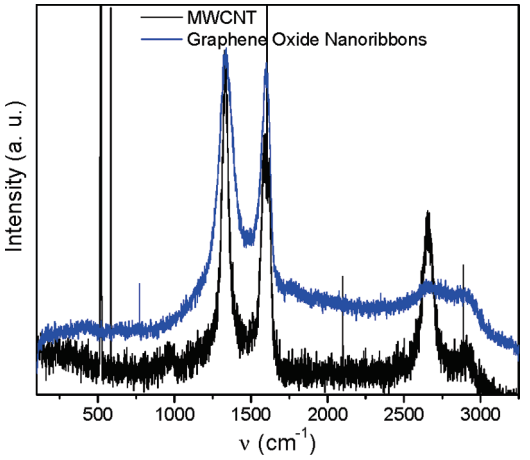

Figure 2. Raman spectroscopic image of graphene oxide nanoribbons compared to the carbon MWNT feedstock used to produce the graphene oxide nanoribbons. The lack of a sharp peak around 2637 cm^{-1} indicates that the chemical unzipping process is completed, as other work on graphene nanoribbons shows the same characteristic lack of peak.[15]

MWNTs (Figure 2). This is in good agreement with the previous results for the unzipping process published by Tour.[15]

To confirm the reduction of the GNRs, XRD measurements using Cu Kα radiation were conducted. The diffraction pattern of the pristine carbon MWNTs (Figure 3) showed a peak at $2\theta \approx 25.8°$ that corresponds to a d-value of ∼3.4 Å, which is typical for the interwall separation distance for MWNTs. The lowest angle diffraction peak after chemical unzipping shifts to $2\theta = 9.7°$ (d-value about 9.1 Å), corresponding to the (002) reflection from intercalated stacked graphite oxide sheets.[16] The shift is a consequence of the presence of oxygen-containing functional groups after the highly oxidative unzipping processes, which in turn enables intercalation of solvent and water molecules, thereby further increasing the distance between partially stacked graphene oxide nanoribbons. The absence of the peak at $2\theta \approx 25.8°$, corresponding to the interwall separation within carbon MWNTs, evidences a high degree of unzipping. After reduction of the graphene oxide nanoribbons, using both hydrazine and thermal annealing, there is demonstrable conversion of graphene oxide nanoribbons to partially stacked graphene nanoribbons, as shown in the XRD patterns of Figure 3.

Figure 4A shows the absorption and emission profile of the GNRs used in this work. We observe the onset of photoluminescence of the GNRs around 350 nm, which agrees with the emission peaks observed for synthetic 2D graphene nanoribbons[18] and is similar to those for ultrasonicated graphene oxide flakes[19] (350 nm). This onset is roughly at the same energy at which I_3^- in acetonitrile has been reported to absorb light.[2] Figure 4B gives a comparison of the light absorption of I^- and I_3^- in a solution of acetonitrile overlaid with the emission spectrum of the few-layer graphene nanoribbons, showing the spectrum of light that the redox couple absorbs as compared to the emission profile. The absorption of the I_3^- shows a strong overlap with the emission spectrum of the few-layer graphene nanoribbons, which is essential for FRET.

There are two alternative explanations for the mechanism of photoluminescence in the literature for graphene and few-layer stacks of graphene. Chhowalla et al.[19] suggest that this blue photoemission is due to the formation of small domains of polycyclic aromatic hydrocarbon fragments (i.e., graphene quantum dots) within sp^3-containing carbon matrixes. The presence of these π-conjugated islands arises between regions of remaining functional groups containing oxygen atoms that are present at both sheet surfaces and sheet edges. This would require a very small amount of functional groups left on the ribbons, as the XRD test had no peak at $2\theta = 9.7°$, which is used for indicating graphene oxide sheets. A second possible explanation involves the effect of the nanoribbon width on nanoribbon photoluminescence. However, the calculated band gap[20] for our ~10 nm wide graphene nanoribbons (Figure 1B) is ~0.1 eV, which is smaller than the 2.5−3.5 eV range of the observed fluorescence (Figure 4). To fit the theory, we can assume a degree of isolation between the layers of the graphene nanoribbons and then attribute the emission response to thinner ribbons that arise from unzipping the inner shells of the multiwalled carbon nanotubes. This would give photoluminescence emission in the observed range, as would defect sites on the nanotube ribbons that correspondingly limit conjugation.

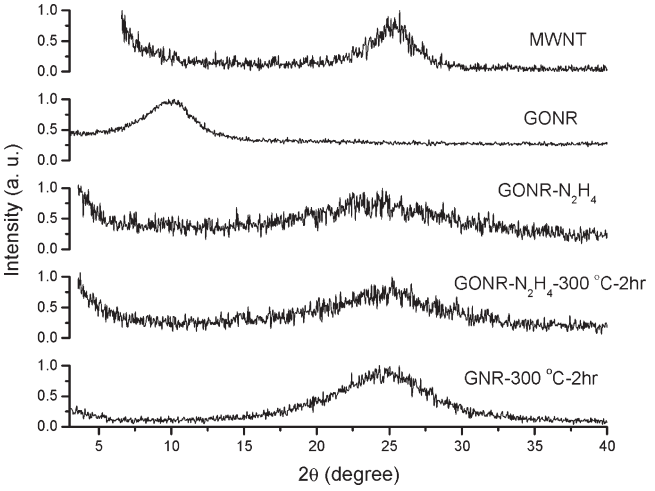

Figure 3. XRD patterns of the carbon MWNTs, few-layer graphene oxide nanoribbons (GONRs), and GNRs produced from GONRs by reduction with hydrazine, thermal reduction, or both hydrazine and thermal reduction.

Figure 5 shows UV−vis transmission measurements for a DSSC cell with a dye-free TiO_2 photoelectrode and a few-layer graphene nanoribbon counter electrode when using a 1.5 V bias to simulate the driving potential of the absent dye and I^-/I_3^--containing acetonitrile electrolyte. As shown here, dramatic bleaching of the absorption in the 380−500 nm range for I_3^- in acetonitrile occurs when the cell is exposed to AM 1.5 light. When compared to Figure 4B, Figure 5 shows that it is the change in the absorbance of the I_3^- component of the electrolyte that corresponds well to the change in transparency of the total cell under testing. Another significant aspect of the transparency test under light stimulation and electrical bias is that there is a slight decrease in transparency for longer wavelengths of visible light, which is also attributed to the use of GNRs shifting the absorption spectra of the I_3^- to longer wavelengths at the edge of or outside the visible region of light. This overall effect seems to be a trade-off of having increased transparency in the optical range for decreased transparency in the near-IR range. This is

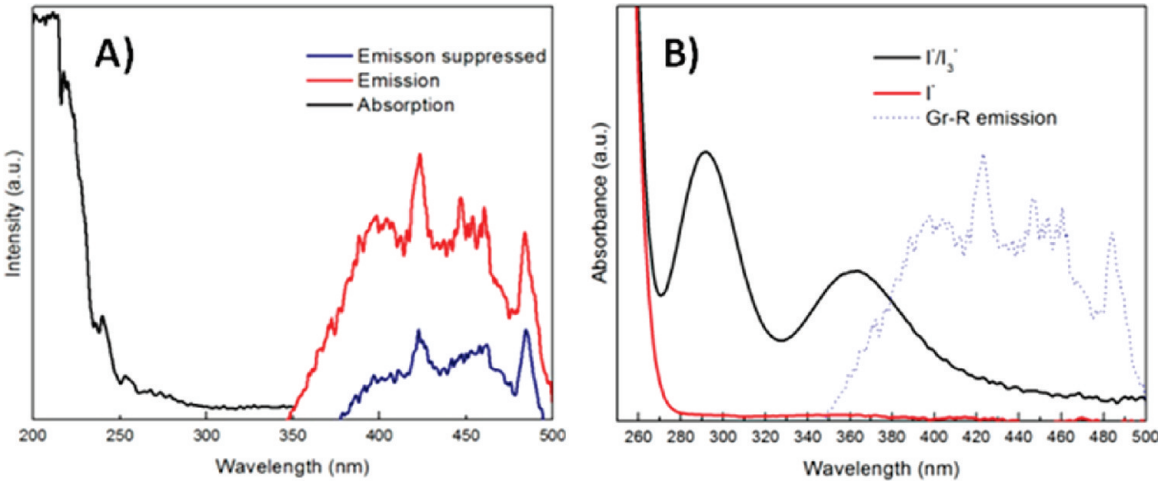

Figure 4. (A) Black and red curves show the absorption and emission spectra from GNRs drop-cast on a quartz slide and inserted into a cuvette containing acetonitrile. The blue curve shows the suppressed emission from an identically prepared sample of GNRs exposed in a cuvette to an acetonitrile solution containing 0.6 M I^- and 0.03 M I_3^-. The emission data were obtained using $\lambda = 280$ nm excitation. (B) Absorption spectra of I^- and I/I_3^- in a solution of acetonitrile, with an overlay of the emission pattern of the graphene nanoribbons (dotted line) which shows very good agreement with the change in overall device transparency in Figure 5, showing that this energy transfer specifically affects the I_3^-.

dx.doi.org/10.1021/jp2069946 |J. Phys. Chem. C 2011, 115, 25125–25131

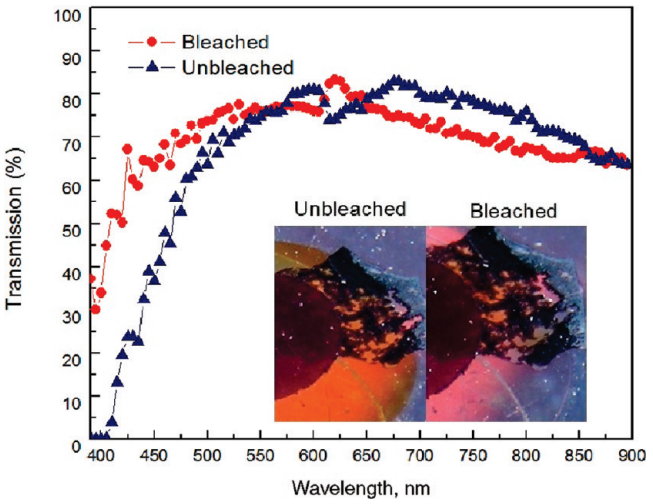

Figure 5. UV−vis transmission measurements for a DSSC cell with a dye-free TiO_2 photoelectrode and a few-layer graphene nanoribbon counter electrode when using a 1.5 V bias to simulate the driving potential of the absent dye. The electrolyte in the cell is composed of a 0.6 M I^- and 0.03 M I_3^- redox couple in acetonitrile. Transmission spectra are shown for before and after exposure to AM 1.5 light. Inset: Optical pictures comparing unbleached and photobleached electrolyte in a working cell. The red color region observed in the bleached electrolyte is the sample holder, which under the photobleached state is readily visible through the electrolyte.

Scheme 1. Two Main Possible Reaction Paths of How Photobleaching May Occur[a]

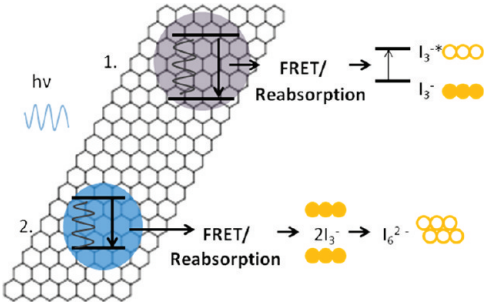

[a] The first is that stimulated triiodide is formed (I_3^{*-}) under FRET/reabsorbtion from the graphene nanoribbons possessing a modified outer valence shell, leading to modified absorption. The second possibility is that in its excited state the triiodide may bond with other iodine ions to form a higher polyiodide, which we represent here with two triiodides forming a hexaiodide (I_6^{2*-}).

advantageous for the dye solar cell because of the sensitivity range of the currently available dyes, which have a much stronger spectral response in the visible range.

The inset of Figure 5 shows photographs comparing the color of the electrolyte in the above DSSC when light is not shining on the cell and after a 1 min exposure of the cell to AM 1.5 simulated light. The color transition takes place over the course of 1 min when the DSSC is situated in a connected circuit under the light.

We propose that this electrolyte photobleaching is triggered by the photostimulation of regions of π-conjugated graphene quantum-dot-like regions in the nanoribbons. From Figure 4B we have shown that there is an overlap between the emission of

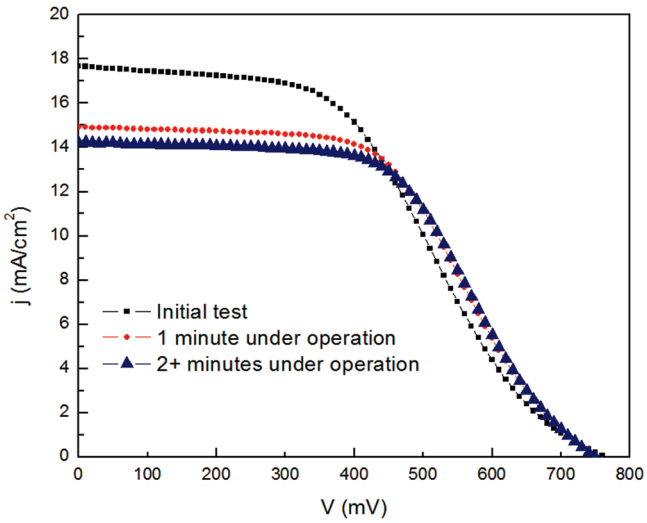

Figure 6. DSSC $I-V$ test results as a function of the exposure time (AM 1.5 at 100 mW/cm^2) when using a graphene nanoribbon counter electrode. The results are for the initial cell, the cell exposed for 1 min, and the cell exposed for 2 min, after which the cell response was unaffected by further light exposure.

Table 1. Summary of the Data in Figure 6 for the Initial Current−Voltage Evaluation and after Exposure to AM 1.5 for 1 and 2 min[a]

time	U_{oc}, mV	I_{sc}, mA/cm^2	FF	efficiency
initial	770	17.68	0.45	6.06
1 min	760	14.908	0.52	5.94
2 min	750	14.225	0.55	5.83

[a] U_{oc} is the open circuit potential, I_{sc} is the short circuit current, and FF is the fill factor.

the GNRs and the absorption of the I_3^-, implying that the mechanism behind this is an energy transfer effect, whether it is a FRET or a photon reabsorption, from the graphene ribbon to the triiodide that yields an ion structure less absorbing in the optical range of light. Scheme 1 discusses the two routes to this alternative ion structure, where FRET or photon reabsorption, depending on the range of the interaction, alters the triiodide to produce these new optical properties. Whether it is through FRET or photon reabsorption, this effect leads to an altered absorption of light from the changes effected to the I_3^- component of the redox couple. It is entirely possible that the photostimulated I_3^- may form more metastable polyiodides such as a I_6^- ion, which warrants further testing.

In terms of practical operation of the DSSC using GNRs at the counter electrode, there is a transient behavior of the performance of the DSSC. Initially, there is a high I_{sc} current density of 17.9 mA/cm^2 and a lower than expected fill factor of 0.45 in the DSSC. However, over the course of repeated tests, after 2 min in the solar simulator, the solar cell drops in current density to a steady state I_{sc} of 14.2 mA/cm^2 and increases in fill factor to 0.55, giving little net change in the overall power conversion efficiency. Furthermore, this entire process is completely reversible; stopping photoexposure of the DSSC causes the electrolyte to revert to its expected color in about the same time as it takes for bleaching to full transparency. If the DSSC is then placed under the simulated light, the same transition from high current density

dx.doi.org/10.1021/jp2069946 |J. Phys. Chem. C 2011, 115, 25125–25131

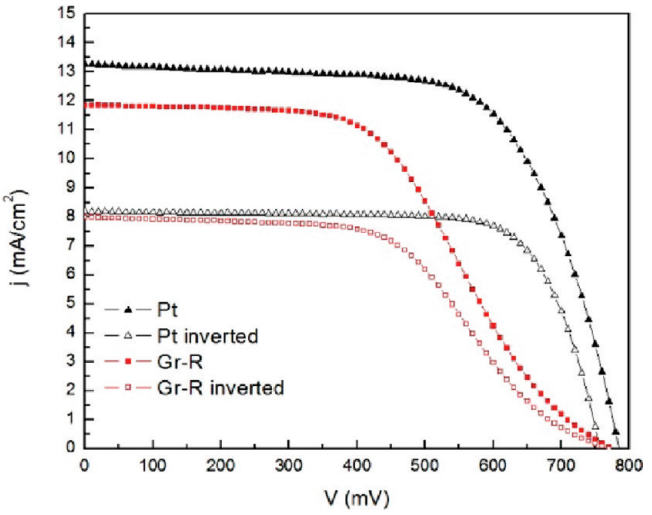

Figure 7. $I-V$ results (under simulated AM 1.5 at 100 mW/cm^2) for DSSCs based on a semitransparent Pt counter electrode and a counter electrode of graphene nanoribbons. Results are shown for both the standard configuration (solid shapes) and the inverted configuration (hollow shapes), where light is shined through the counter electrode and electrolyte before reaching the photoanode.

Table 2. Chart Summarizing the Data in Figure 7 for the Standard Configuration and the Inverted Configuration for DSSCs Based on Both Platinum and Graphene Nanoribbon Electrodes

counter electrode	U_{oc}, mV	I_{sc}, mA/cm^2	FF	efficiency
Pt reference	790	13.269	0.662	6.93
inverted Pt	760	8.183	0.745	4.63
graphene ribbons	780	11.852	0.499	4.61
inverted ribbons	770	7.983	0.525	3.23

and low fill factor to lower current density and higher fill factor is again observed.

Figure 6 and Table 1 show data on the operation of a dye solar cell that uses graphene nanoribbons in the counter electrode in an initial test, after 1 min of operation, and after 2 min of operation. Further $I-V$ testing of the DSSC after 2 min under the light source gave the same results as the test at 2 min, indicating completion of the photobleaching process.

Recently, graphitic materials have been successfully used as conductive and optically transparent counter electrode catalysts in dye solar cells.[21] This idea, combined with the photoinduced optically transparent electrolyte shown herein, offers advantages for two different applications of DSSCs. The first application is to improve the operation of inverted DSSCs, where light is shined through a semitransparent counter electrode and through the bulk electrolyte before it reaches the photoanode. The purpose of this geometry is that it is possible to situate the photoanode on an opaque substrate, such as steel or titanium foil, which is of lower cost and more easily processed[3] than standard DSSCs using FTO glass. The second possible application for this increased optical transparency is in a tandem device in which the DSSC is a top cell, where the increased transparency allows more light to pass through the top cell to underlying cells.[4] Figure 7 and Table 2 compare performance results for semitransparent DSSCs using

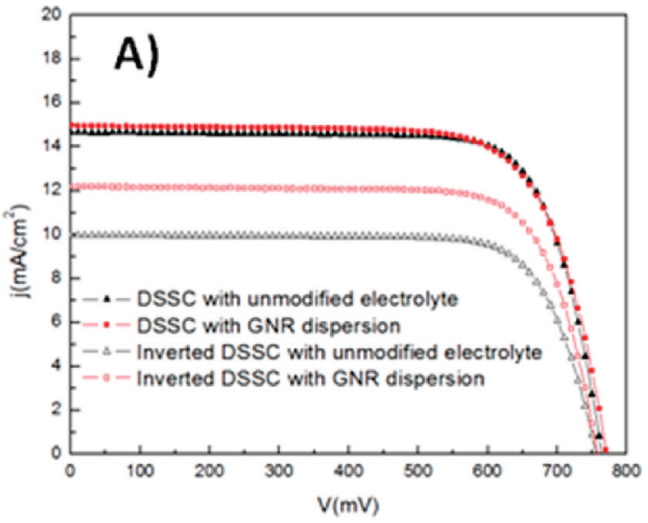

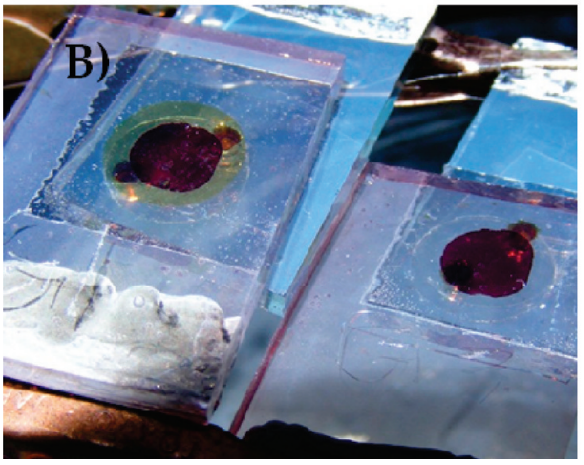

Figure 8. (A) DSSCs with few-layer graphene nanoribbons dispersed into the electrolyte compared to a standard DSSC containing no few-layer graphene nanoribbons. Results are shown for both the standard configuration (solid shapes) and the inverted configuration (hollow shapes), where light is shined through the counter electrode and electrolyte before reaching the photoanode. (B) Side by side comparison photo of DSSCs with unmodified electrolyte (left) and electrolyte with GNRs dispersed into it (right) when both are under photostimulation.

Table 3. Summary Chart of $I-V$ Characterization in Figure 8

cell	U_{oc}, mV	I_{sc}, mA/cm^2	FF	efficiency
DSSC with unmodified electrolyte	770	14.682	0.754	8.53
DSSC with GNR dispersion	780	14.973	0.721	8.43
inverted DSSC with unmodified electrolyte	760	9.984	0.758	5.75
inverted DSSC with GNR dispersion	760	12.185	0.757	7.01

either platinum or graphene nanoribbons as the counter electrode. Comparison for both cell types is for the standard orientation and an inverted orientation in which light must propagate through the counter electrode and electrolyte before reaching the photosensitive dye/mesoporous TiO_2 electrode.

dx.doi.org/10.1021/jp2069946 |J. Phys. Chem. C 2011, 115, 25125–25131

While the overall power conversion of the reference platinum solar cell is higher than for the graphene ribbon solar cell (with power conversion efficiencies of 6.93% and 4.61%, respectively, for the standard configuration), the performance loss on shining light through the counter electrode in the inverted configuration is smallest when using the graphene nanoribbon coated counter electrode. In a performance comparison for standard versus inverted orientation, a loss of ~3.8 mA/cm^2 (32%) is seen when shining light through a steady-state-operating graphene nanoribbon DSSC versus the current density loss of 5.1 mA/cm^2 (38%) when using a Pt counter electrode.

For a direct comparison of the increase in photocurrent from the use of few-layer graphene nanoribbons in the photobleaching electrolyte, a third test was performed in which standard DSSCs with platinum counter electrodes were used and some cells made use of an electrolyte where graphene nanoribbons were suspended by ultrasonication into the electrolyte directly. The concentration of graphene nanoribbons in the electrolyte after ultrasonication and removal of the unsuspended few-layer graphene ribbons was 0.04 mg/mL. It is suspected that using a gelation agent, such as poly(vinylidene fluoride-*co*-hexafluoropropylene) (PVDF-HFP)[22] or silica nanoparticles,[23] would allow for a greater loading of the graphene into the electrolyte and a consequently greater photobleaching response. Even within the limitation of only a minimal amount of graphene nanoribbons, an incomplete photobleaching of the electrolyte occurred, with a small but significant increase in the photocurrent of the optically inverted DSSCs containing the graphene nanoribbons suspended in the electrolyte. Figure 8 and Table 3 show a summary of the results, where a DSSC in the standard versus optically inverted orientation goes from an I_{sc} of 14.682 mA/cm^2 to an I_{sc} of 9.984 mA/cm^2 (31.9% loss of photocurrent) for the reference cell and from an I_{sc} of 14.973 mA/cm^2 to an I_{sc} of 12.185 mA/cm^2 (18.6% loss of photocurrent) using the electrolyte containing the few-layer graphene ribbons. This difference is an increase of 21.9% in power conversion efficiency found chiefly through the increase in photocurrent from photobleaching of the electrolyte, demonstrating the potential of using the few-layer graphene nanoribbons as an additive material to the electrolyte and also supporting the idea that the graphene nanoribbons are stimulating to the triiodide in the electrolyte by FRET rather than a charge transfer process. Since the GNRs are electrically isolated from the circuit when suspended in the electrolyte, it is unlikely that a sustained process with electron transfer from the GNRs to the electrolyte will happen.

4. CONCLUSION

In conclusion, a surprising, highly reversible photobleaching effect was observed for the iodide/triiodide redox couple when using a graphene nanoribbon counter electrode. This effect has not been reported for other nanocarbons, including carbon nanotubes, carbon black, and other forms of graphene. While the photobleaching does not affect the power conversion efficiency for the standard cell configuration, it does improve the fill factor under operation and decreases the photocurrent of the cell. Most importantly, this photobleaching and resulting decrease of electrolyte absorption improves significantly the performance of the tested inverted configuration, with the mesoporous titania/dye photoelectrode at the bottom where light propagates through the electrolyte and cathode to reach the photoelectrode. Hence, this photobleaching effect provided by few-layer graphene nanoribbons can be used advantageously for structurally inverted dye solar cells and for tandem solar cells.

AUTHOR INFORMATION

Corresponding Author

*E-mail: zakhidov@utdallas.edu.

ACKNOWLEDGMENT

This work was supported through the Rice/Air Force Research Lab (AFRL) CONTACT program on tandem solar cells, Welch Program AT-1617, and Robert A. Welch Foundation Grant AT-0029.

REFERENCES

(1) O'Regan, B.; Gratzel, M. *Nature* **1991**, *353* (6346), 737–740.
(2) Kebede, Z.; Lindquist, S.-E. *Sol. Energy Mater. Sol. Cells* **1999**, *57* (3), 259–275.
(3) Ito, S.; Ha, N.-L. C.; Rothenberger, G.; Liska, P.; Comte, P.; Zakeeruddin, S. M.; Pechy, P.; Nazeeruddin, M. K.; Gratzel, M. *Chem. Commun.* **2006**, *38*, 4004–4006.
(4) Liska, P.; Thampi, K. R.; Gratzel, M.; Bremaud, D.; Rudmann, D.; Upadhyaya, H. M.; Tiwari, A. N. *Appl. Phys. Lett.* **2006**, *88* (20), 203103–203103−3.
(5) Feldt, S. M.; Gibson, E. A.; Gabrielsson, E.; Sun, L.; Boschloo, G.; Hagfeldt, A. *J. Am. Chem. Soc.* **2010**, *132* (46), 16714–16724.
(6) Gregg, B. A.; Pichot, F.; Ferrere, S.; Fields, C. L. *J. Phys. Chem. B* **2001**, *105* (7), 1422–1429.
(7) Wang, M.; Chamberland, N.; Breau, L.; Moser, J.-E.; Humphry-Baker, R.; Marsan, B.; Zakeeruddin, S. M.; Grätzel, M. *Nat. Chem.* **2010**, *2* (5), 385–389.
(8) Suzuki, K.; Yamaguchi, M.; Kumagai, M.; Yanagida, S. *Chem. Lett.* **2003**, *32* (1), 28–29.
(9) Ramasamy, E.; Lee, W. J.; Lee, D. Y.; Song, J. S. *Electrochem. Commun.* **2008**, *10* (7), 1087–1089.
(10) Roy-Mayhew, J. D.; Bozym, D. J.; Punckt, C.; Aksay, I. A. *ACS Nano* **2010**, *4* (10), 6203–6211.
(11) Murakami, T. N.; Ito, S.; Wang, Q.; Nazeeruddin, M. K.; Bessho, T.; Cesar, I.; Liska, P.; Humphry-Baker, R.; Comte, P.; Pechy, P.; Gratzel, M. *J. Electrochem. Soc.* **2006**, *153* (12), A2255–A2261.
(12) Yu, Z.; Gorlov, M.; Nissfolk, J.; Boschloo, G.; Kloo, L. *J. Phys. Chem. C* **2010**, *114* (23), 10612–10620.
(13) Huang, S. Y.; Schlichthörl, G.; Nozik, A. J.; Grätzel, M.; Frank, A. J. *J. Phys. Chem. B* **1997**, *101* (14), 2576–2582.
(14) Zhang, M.; Fang, S.; Zakhidov, A. A.; Lee, S. B.; Aliev, A. E.; Williams, C. D.; Atkinson, K. R.; Baughman, R. H. *Science* **2005**, *309* (5738), 1215–1219.
(15) Kosynkin, D. V.; Higginbotham, A. L.; Sinitskii, A.; Lomeda, J. R.; Dimiev, A.; Price, B. K.; Tour, J. M. *Nature* **2009**, *458* (7240), 872–876.
(16) Higginbotham, A. L.; Kosynkin, D. V.; Sinitskii, A.; Sun, Z.; Tour, J. M. *ACS Nano* **2010**, *4* (4), 2059–2069.
(17) Park, S.; An, J.; Jung, I.; Piner, R. D.; An, S. J.; Li, X.; Velamakanni, A.; Ruoff, R. S. *Nano Lett.* **2009**, *9* (4), 1593–1597.
(18) Yang, X.; Dou, X.; Rouhanipour, A.; Zhi, L.; Räder, H. J.; Müllen, K. *J. Am. Chem. Soc.* **2008**, *130* (13), 4216–4217.
(19) Eda, G.; Lin, Y.-Y.; Mattevi, C.; Yamaguchi, H.; Chen, H.-A.; Chen, I. S.; Chen, C.-W.; Chhowalla, M. *Adv. Mater.* **2010**, *22* (4), 505–509.
(20) Son, Y.-W.; Cohen, M. L.; Louie, S. G. *Phys. Rev. Lett.* **2006**, *97* (21), 216803.
(21) Kavan, L.; Yum, J. H.; Grätzel, M. *ACS Nano* **2010**, *5* (1), 165–172.
(22) Wang, P.; Zakeeruddin, S. M.; Moser, J. E.; Nazeeruddin, M. K.; Sekiguchi, T.; Gratzel, M. *Nat. Mater.* **2003**, *2* (6), 402–407.
(23) Wang, P.; Zakeeruddin, S. M.; Comte, P.; Exnar, I.; Grätzel, M. *J. Am. Chem. Soc.* **2003**, *125* (5), 1166–1167.